Efficient non-reflecting boundary condition constructed via optimization of damped layers

Reese E. Jones[1,*] and Christopher J. Kimmer[2,†]
[1]*Mechanics of Materials Department, Sandia National Laboratories, Livermore, California 94551-0969, USA*
[2]*Computer Engineering and Computer Science Department, University of Louisville, Louisville, Kentucky 40292, USA*
(Received 10 December 2009; published 5 March 2010)

In this work we use analytic and numerical techniques to construct optimal, nearly reflectionless boundary layers for lattice dynamics by tuning the mass, stiffness, and damping of those layers. Using a one-dimensional nearest-neighbor chain as a model system, we obtain analytical results for the low and high-frequency behavior of such boundary conditions, as well as a continued fraction solution for the reflection coefficient of multiple layers. In addition, we obtain optimal parameters for the one-dimensional system and a three-dimensional system using wave packets with normal incidence and compare the results to an implementation of the exact boundary condition in one dimension and optimal versions of the commonly used ramped damping in three dimensions.

DOI: 10.1103/PhysRevB.81.094301 PACS number(s): 45.10.−b, 02.70.Ns, 62.30.+d

I. INTRODUCTION

The need for reflectionless boundary conditions is clear in any simulation involving waves in a domain that is necessarily finite due to computational resources. Many treatments have been developed for waves in continuous media, e.g., acoustics and elasticity[1] as well as electromagnetics.[2] Here, we are concerned specifically with discrete lattice dynamics and our goal is to develop tuned, computationally inexpensive, easy-to-implement nonreflecting boundary conditions for molecular dynamics (MD) and MD-based multiscale applications that avoids storage of the history of the atomic trajectories and the computation of convolution integrals.

The form of an exact reflectionless boundary condition is known. Adelmann and Doll[3] derived a generalized Langevin equation based on a continued fraction representation[4] that is the exact solution to the problem of reflectionless wave propagation in a semi-infinite one-dimensional (1D) chain of atoms. This treatment involves a convolution of a system-dependent kernel with the history of atomic displacements or velocities near the boundary of the system and was subsequently called the time history kernel (THK) when used in multiscale applications.[5] The THK is the optimal solution for propagation in linear media and, with perfect precision arithmetic and an arbitrarily long history, it is reflectionless. For more complex, three-dimensional (3D) systems the kernel can be determined numerically[6] or analytically,[7] although evaluation of the analytical expressions for typical 3D systems remains a challenge. In all cases, the kernel unfortunately has a very slow and oscillatory decay in time and therefore is very expensive computationally.

E and co-workers were apparently the first to form an optimal approximate boundary condition in order to increase efficiency.[8] With their variational boundary condition (VBC), they generalized the problem to finding the optimal coefficients of a finite kernel. The particular form of the VBC subsumes the THK and allows for trade-offs in the length of kernel history versus the number of boundary layers.[9] The coefficients of the terms that comprise the kernel, which is nonlocal in time and space, are derived based on the minimization of the reflection coefficient across the Brillouin zone. In their perfectly matched multiscale simulation (PMMS) method,[10,11] Li and co-workers took an alternate approach by forming the discrete analog to the well-known perfectly matched layer (PML) of continuum wave propagation.[2] The discrete PML (Ref. 11) and its extension MD-PML,[12] attempt to create a reflectionless boundary layer by employing complex-valued elastic constants that vary in space. The change in elastic properties allows one to tune the impedance of the boundary condition while introducing dissipation through the damping caused by the imaginary parts of the constants. In the simplest versions of the PMMS method, the impedance matching is not exact although the boundary condition is local in time and consequently relatively simple to implement in existing MD frameworks. However, the method is predicated on determining an optimal damping function which, to date, has not been determined; only *ad hoc* forms of this function have been used. The MD-PML method more closely matches the impedance of the original MD system at the cost of a considerably more complicated, coupled dynamics in the region where the boundary condition is applied. Comparative studies of the various methods can be found in the literature.[9,11,13]

Our proposed method is also motivated by finding an efficient, optimal approximate boundary condition using essentially the same objective function as Li and E,[9] namely, the obvious one of minimum average reflection coefficient over a range of frequencies.[24] Unlike E and co-workers we limit ourselves to multilayer treatments that are local in time, i.e., no storage of history nor convolution, in an effort to produce a method that could be applied in an MD simulation without modification of the underlying code. For instance, the proposed method was constructed in the well-known LAMMPS code[14] without modification. It relies on treating the mass, damping constant, and stiffnesses of atoms participating in the boundary condition as parameters which may be varied to optimize the reflection coefficient. The optimization process we employed is a combination of analytical and numerical methods for simpler systems and is fully numerical for more complex systems. To this end, we present results yielding an analytic expression for the reflection coefficient as a function of frequency for an arbitrary boundary condition in a 1D harmonic chain. Moreover, we introduce the use of

multiple Gaussian wave packets in a single MD simulation as a new method for determining the frequency response of the boundary condition. Given the free parameters and dynamics of our simple one-dimensional model system, the boundary layer can be interpreted as a sequence of second order filters. In this context, we observe that the optimal layer is constructed by evenly spacing the zeros of the reflection function in the frequency range of interest.[25] This effects a collocation of the reflection function to zero at specific frequencies.

In Sec. II, we summarize early results for reflection in 1D systems and present analytical results that represent a considerable generalization of the previous analysis.[15] These expressions are used to derive the behavior of a general boundary condition in the high- and low-frequency limits. In Sec. III, we put the boundary treatment into practice and apply our numerical optimization scheme. We give some rationale for choosing among the various permutations the modified damped layer can have, i.e., modification of mass; spring stiffness, either per atom or per bond; and damping, either per atom or per bond. With 1D simulation results based on a discrete sampling of the reflection spectrum using wave packets, we are able to show good correspondence with the novel analytical results. Then we apply the same methodology to a 3D system with a more complex lattice and introduce the multiple wave-packet method for MD as a novel means to efficiently quantify the behavior of a specific boundary condition. We conclude with discussion of future work including the treatment of general three-dimensional problem where normal incidence on a planar boundary is not assumed.

II. 1D CHAIN ANALYSIS

The model system we consider for analytical treatment is a monatomic, harmonic 1D chain with mass m, nearest-neighbor interactions, and spring constant κ. The equation of motion for atom n in the chain, with displacement u_n, is given by

$$m\ddot{u}_n = \kappa(u_{n+1} + u_{n-1} - 2u_n), \tag{1}$$

whose Fourier transform determines the dispersion relation

$$\omega(k)^2 = 2\omega_0^2(1 - \cos(ka)) = \omega_{\max}^2 \sin^2\left(\frac{1}{2}ka\right), \tag{2}$$

with the maximum frequency twice the natural frequency of a bond: $\omega_{\max} = 2\sqrt{\frac{\kappa}{m}} \equiv 2\omega_0$. Here a is the lattice constant. Periodic boundary conditions allow one to guess that the steady state solution is the real part of

$$u_n = A_i e^{i(kna - \omega t)}, \tag{3}$$

where A_i is a complex amplitude determining the overall phase of the wave and the energy in the wave (which is proportional to $|A_i|^2\omega^2$). The velocity is simply the real part of $v_n = -i\omega u_n$.

A. Reflectionless boundary condition

As mentioned in the Introduction, the THK (Ref. 3) is a linear operator on the velocity or displacement history. It effects the linear response of semi-infinite lattice and, consequently, it is a perfectly reflectionless boundary condition for small amplitude waves. The THK is derived by separating an infinite one-dimensional chain into two parts, the explicit ($n \leq 0$) and the implicit ($n > 0$); solving, with transforms, for the trajectories of the implicit half in terms of the trajectories of the explicit half; and then substituting these equations in the equations of motion of the explicit atoms to eliminate unwanted degrees of freedom as in the Mori-Zwanzig formalism.[16] For a nearest-neighbor one-dimensional chain, the equation for the last explicit atom (index $n=0$) is

$$m\ddot{u}_0 = \kappa(u_{-1} - u_0) + \int_0^t \theta(t-\tau)u_0(t)d\tau + r = \kappa(u_{-1} - u_0) + \kappa u_0 - \int_0^t \beta(t-\tau)\dot{u}_0(t)d\tau + r_\beta, \tag{4}$$

where the kernels are: $\theta(t) = -\frac{2\kappa}{t}J_2(2\omega_0 t) = \dot{\beta}(t)$, and $\beta(t) = \frac{\kappa}{\omega_0 t}J_1(2\omega_0 t)$. Here, J_1 and J_2 are the first-order and second-order Bessel functions of the first kind, respectively. Note that the terms, $r = \theta(t)\dot{u}_1(0) - \dot{\theta}(t)u_1(0)$ and $r_\beta(t) = r(t) + \beta(t)\ddot{u}_1(0)$, that collect the initial conditions are zero if the removed part of the chain is quiescent at $t=0$.[26] The approach we consider in this work essentially amounts to simplifying the history kernel while not treating the initial conditions, which are temperature dependent. Consequently, any available method in the literature of treating the finite-temperature effects in these terms could potentially be used without modification in our method. Here we define

$$\bar{\beta} = \int_0^\infty \beta(t)dt = \frac{\kappa}{\omega_0}, \tag{5}$$

and note that $\beta(0) = \kappa$. For a linear chain with a quiescent start, Eq. (4) reduces to

$$m\ddot{u}_0 = \kappa(u_1 - u_0) - \bar{\beta}\int_0^t \frac{1}{t-\tau}J_1[2\omega_0(t-\tau)]\dot{u}_0(\tau)d\tau. \tag{6}$$

It is often approximated as

$$m\ddot{u}_0 = \kappa(u_1 - u_0) - \bar{\beta}\dot{u}_0, \tag{7}$$

to avoid the convolution integral.

In practice, the integral in Eq. (4) needs to be approximated by a quadrature based on the discrete time history of the numerical integrator

$$m\ddot{u}_0(i\Delta t) = \kappa[u_1(i\Delta t) - u_0(i\Delta t)] - \bar{\beta}\sum_{j=0}^{\min(N,i-1)} \frac{1}{i-j}J_1[2\omega_0\Delta t(i-j)]\dot{u}_0(j\Delta t), \tag{8}$$

where Δt is the time step and the current time $t = i\Delta t$. As we see in Fig. 1, the performance of the THK truncated at a finite length degrades with decreasing kernel size N and eventually behaves like a simple damped boundary condition. Here we have defined the reflection coefficient as the ratio of reflected energy to incident energy as a function of frequency of the incident waveform. It is also noteworthy

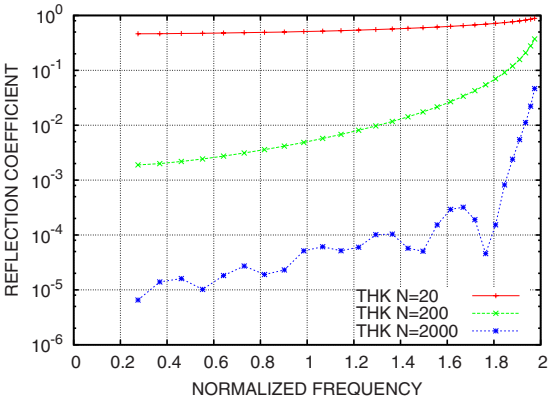

FIG. 1. (Color online) Comparison of the (energy) reflection coefficient as a function of frequency for truncated, finite THKs of varying convolution length. Frequencies have been normalized by ω_0.

that the high-frequency response is considerably worse than the low-frequency response. Finally, we remark that this boundary condition in 1D requires storage of order N and additional floating point operations of order N at each time step. Moreover, as the timestep Δt is decreased, N must be increased in inverse proportion to Δt in order to achieve similar performance to the $N=2000$ case pictured here. In three dimensions, the scaling is the same, although the absolute storage required and computational expense is greater. In contrast, the method we propose below is independent of the time step and requires additional storage and computation of order the number of boundary layers used, which will typically be a much smaller integer than the history kernel length.

B. Interfaces

An imperfect boundary condition will inevitably create a change of impedance at the interface between the explicit region $n<0$ where the dynamics are important and the implicit region $n\geq 0$ which tries to mimic a semi-infinite chain. Scattering off an interface between regions with different force constants has been solved algebraically. For an interface at $n=0$ between regions with force constants κ and κ_+ Eq. (1) becomes

$$m\ddot{u}_n = \kappa(u_{n+1} + u_{n-1} - 2u_n), \quad n < 0, \tag{9}$$

$$m\ddot{u}_0 = \kappa(u_{-1} - u_0) + \kappa_+(u_1 - u_0), \tag{10}$$

$$m\ddot{u}_n = \kappa_+(u_{n+1} + u_{n-1} - 2u_n), \quad n > 0. \tag{11}$$

The solution to these equations was first presented in the literature by Steinbrüchel,[15] whose approach we summarize here. For an incident wave traveling from negative n in the direction of increasing n, the ansatz is

$$u_n = e^{i(k_i na - \omega_i t)} + Re^{i(k_r na - \omega_r t)}, \quad n < 0, \tag{12}$$

$$u_n = Te^{i(k_t na - \omega_t t)}, \quad n \geq 0. \tag{13}$$

Continuity of displacement and its time derivatives for all times yields the condition

$$\omega_i = \omega_r = \omega_t \equiv \omega, \tag{14}$$

while the dispersion relation for $n<0$ yields

$$k_r = -k_i. \tag{15}$$

The wave vector of the transmitted wave is determined by the condition of equal frequencies using the dispersion relations of the two semi-infinite crystals so that we finally have

$$u_n = e^{i(k_i na - \omega t)} + Re^{i(-k_i na - \omega t)}, \quad n < 0, \tag{16}$$

$$u_n = Te^{i(k_t na - \omega t)}, \quad n \geq 0. \tag{17}$$

Using Eq. (9) for $n=-1$, substituting in the ansatz of Eqs. (16) and (17), and using $m\omega^2 = \kappa(e^{ik_i a} + e^{-ik_i a} - 2)$ yields a statement of displacement continuity at the interface

$$1 + R = T. \tag{18}$$

Equation (10) with similar substitutions of the ansatz and the dispersion relation for the semi-infinite crystal with force constant κ_+ yields

$$T[\kappa_+(e^{ik_t a} - 1) + \kappa] = \kappa(e^{-ik_i a} + Re^{ik_i a}). \tag{19}$$

There are now two Eqs. (18) and (19) in two unknowns, T and R, which give the amplitude of the reflected wave

$$R = \frac{\kappa(1 - e^{-ik_i a}) + \kappa_+(e^{-ik_t a} - 1)}{\kappa(e^{ik_i a} - 1) - \kappa_+(e^{-ik_t a} - 1)}. \tag{20}$$

C. Single boundary layer

A central idea of nonreflecting methods is that the response of a large, effectively semi-infinite region $n\geq 0$ to incoming waves can be approximated by appropriate boundary condition acting on a small portion of this region. To this end, we consider the effect of replacing the semi-infinite region with force constant κ_+ (i.e all $n\geq 0$) by a series of

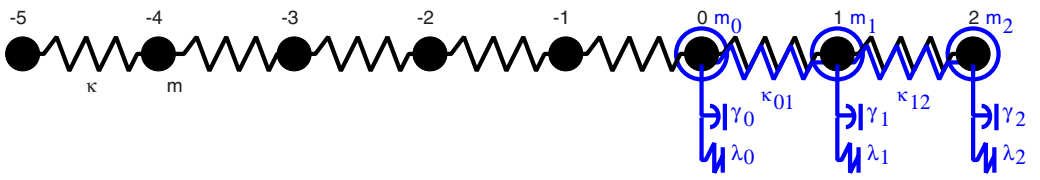

FIG. 2. (Color online) 1D chain of atoms with nearest-neighbor interactions where properties of the atomic layers for $n\geq 0$ have been modified.

so-called "boundary layers" with modified mechanical and elastic properties, see Fig. 2. When these modifications yield linear equations of motion, a similar method to Steinbrüchel's allows the determination of the reflections from this boundary region. For instance, if viscous damping only is applied to this terminating atom at $n=0$ Eq. (10) becomes

$$m_0\ddot{u}_0 = \kappa(u_{-1} - u_0) - \gamma\dot{u}_0. \tag{21}$$

On the other hand, if the boundary atom is also bonded rigidly to a fixed atom, i.e., to maintain the lattice constant and prevent relaxation at the terminating layer, Eq. (10) becomes

$$m_0\ddot{u}_0 = \kappa(u_{-1} - 2u_0) - \gamma\dot{u}_0. \tag{22}$$

Indeed, these equations are specific cases of the general equation of motion

$$m_0\ddot{u}_0 = \kappa(u_{-1} - u_0) + \lambda u_0 - \gamma\dot{u}_0, \tag{23}$$

where an elastic force with force constant λ and a viscous damping force with damping constant γ acts on the boundary particle.

To determine R for these boundary conditions, one recognizes that for an incident wave traveling in the direction of increasing n, the ansatz is unchanged from Eqs. (12) and (13). Substituting the ansatz into the equation of motion for $n=-1$ yields Eq. (18) again so that the displacement of atom 0 is now known in terms of R. Substituting into the equation of motion for $n=0$ and solving for R yields

$$R = \frac{\kappa\left(1 - \frac{m_0}{m}\right)(1 - e^{-ik_i a}) + \kappa\frac{m_0}{m}(e^{ik_i a} - 1) - \lambda - i\omega\gamma}{\kappa\left(1 - \frac{m_0}{m}\right)(e^{ik_i a} - 1) + \kappa\frac{m_0}{m}(1 - e^{-ik_i a}) + \lambda + i\omega\gamma}. \tag{24}$$

In the case where $m_0=m$ and for the specific ω that satisfies $\lambda+i\omega\gamma=-\kappa_+(e^{-ik_i a}-1)$, the boundary condition has matched the impedance of the semi-infinite region with lattice constant κ and Eqs. (20) and (24) are equivalent expressions. Only for this particular frequency will the boundary condition have a zero reflection coefficient $R(\omega)=0$.

For a multiscale simulation, the response of the boundary to long wavelength (i.e., continuum scale) excitations may be of particular concern. In the limit of zero frequency, $e^{\pm ik_i a} \sim 1 \pm i\omega ca$ where $c \equiv a\omega_0$ is the speed of sound in the 1D material. Equation (24) becomes

$$R = \lim_{\omega\to 0} \frac{i\kappa\omega ca - \lambda - i\omega\gamma}{i\kappa\omega ca + \lambda + i\omega\gamma}, \tag{25}$$

indicating that the presence or absence of an elastic force at the boundary governs the long-wavelength response of the boundary *irrespective of the value of the mass* m_0. Specifically, a nonzero elastic force λu_0 leads to $R(\omega=0)=-1$ indicating an inversion of the wave at the boundary while $\lambda=0$ yields a value less than 1 for $\gamma>0$ (i.e., for dissipative damping). Similarly, the short-wavelength, high-frequency limit occurs when $k_i a=-\pi$ and $\omega=\omega_{\max}$ yielding

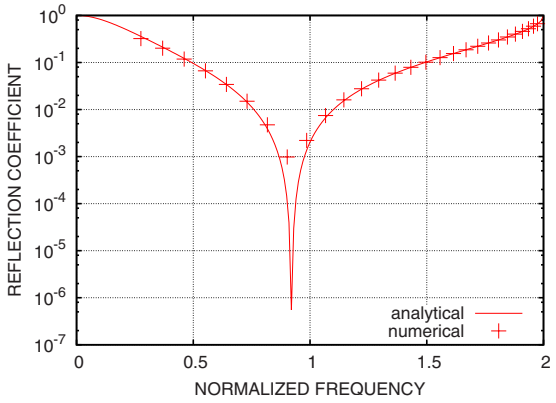

FIG. 3. (Color online) The reflection coefficient R^2 as a function of frequency for a chain with a terminal spring $\lambda=0.4235\kappa$ and damper $\gamma=0.8866\bar{\beta}$, which happens to be the optimal boundary condition of this type. Frequencies have been normalized by ω_0.

$$R = \lim_{\omega\to\omega_{\max}} \frac{2\kappa - 4\kappa\frac{m_0}{m} - \lambda - i\omega\gamma}{-2\kappa + 4\kappa\frac{m_0}{m} + \lambda + i\omega\gamma} = -1. \tag{26}$$

This result shows that complete reflection (accompanied by inversion) of the highest-frequency waves occurs independently of the parameters chosen for the boundary condition.

Figure 3 shows the frequency response of a chain of atoms where the addition of a harmonic well, $\lambda>0$, at the end of the chain creates a zero in $R^2(\omega) \equiv |R(\omega)|^2$ near the middle of the Brillouin zone. We also see that $R^2(0)=1$ and $R^2(\omega_{\max})=1$, as predicted. By examining the form of the THK (6), we see that the stiffness of the THK goes to zero for slow disturbances, i.e., $\omega\to 0$. Clearly, the addition of a harmonic well at the end of the chain does not have this property. The choice of what modifications to the boundary layers are optimal will be treated more fully in Sec. III.

D. Multiple boundary layers

A straightforward extension of Steinbrüchel's method can be used to determine the reflected amplitude for a more general, and more typical, system with a multiple-layer boundary region terminating the chain. However, the algebra quickly becomes cumbersome as the number of boundary layers increases, and one must consider the different dispersion relations accompanying any change in the elastic properties of a layer in the boundary region. Here we show that a simpler method may be used to solve the general problem when one need only determine the value of the reflection coefficient R.

For a series of N damped layers, take the interface between the undamped and damped layers once again to be at $n=0$. The boundary region is specified by the N equations of motion

$$m_0\ddot{u}_0 = \kappa(u_{-1} - u_0) + \kappa_{0,1}(u_1 - u_0) + \lambda_0 u_0 - \gamma_0\dot{u}_0,$$
$$\vdots \tag{27}$$

$$m_n\ddot{u}_n = \kappa_{n,n+1}(u_{n+1} - u_n) + \kappa_{n-1,n}(u_{n-1} - u_n) + \lambda_n u_n - \gamma_n \dot{u}_n,$$

$$\vdots \tag{28}$$

$$m_{N-1}\ddot{u}_{N-1} = \kappa_{N-2,N-1}(u_{N-2} - u_{N-1}) + \lambda_{N-1}u_{N-1} - \gamma_{N-1}\dot{u}_{N-1}. \tag{29}$$

The N layers are considered to have arbitrary bond stiffnesses $\kappa_{i,j}=\kappa_{j,i}$ as well as arbitrary single-body forces (elastic+viscous) and arbitrary masses m_i. In this manner, one has considerable freedom to optimize the boundary condition with respect to these parameters, tailoring it to the desired properties.

For the Steinbrüchel method the ansatz of Eq. (12) is unchanged, recognizing that R is the superposition of the waves reflected at the interface between atom −1 and 0, 0 and 1, 1 and 2, …$N-2$ and $N-1$. Equation (13) is correct for only the terminating atoms and is consequently generalized to the following N ansatzes

$$u_n = T_n e^{i(k_n na-\omega t)} + R_n e^{i(-k_n na-\omega t)}, \quad 0 \le n < N-1, \tag{30}$$

$$u_{N-1} = T_{N-1} e^{i(k_{N-1}(N-1)a-\omega t)}, \tag{31}$$

where it should be noted that the wave with amplitude T_n propagates in the positive x direction and the one with amplitude R_n propagates in negative x. These equations can be solved algebraically; simplifications abound because the phase factors $e^{\pm k_n na}$ always occur as a factor with T_n (upper sign) or R_n (lower sign). However, if one is only interested in R, as is the case here, then the displacements u_n may simply be eliminated beginning with u_{N-1} and ending with u_0 to determine R. For this solution, the initial relation of Eq. (18) is replaced by

$$1 + R = R_0 + T_0, \tag{32}$$

when Eqs. (16) and (30) for $n=0$ are substituted into Eq. (9). Rewriting u_{N-1} in terms of u_{N-2} via Eq. (29) yields

$$u_{N-1} = \frac{\kappa_{N-2,N-1}}{(\kappa_{N-2,N-1} - m_{N-1}\omega^2 - \lambda_{N-1} - i\omega\gamma_{N-1})} u_{N-2} \equiv G_{N-1}u_{N-2}. \tag{33}$$

Indeed, u_n may generally be written in terms of u_{n-1} as

$$u_n = G_n u_{n-1}, \quad 0 \le n \le N-1. \tag{34}$$

The functions G_n are determined from the recurrence relation

$$G_n = \frac{\kappa_{n-1,n}}{(\kappa_{n-1,n} + \kappa_{n,n+1}(1 - G_{n+1}) - m_n\omega^2 - \lambda_n - i\omega\gamma_n)}, \quad 0 \le n < N-1, \tag{35}$$

which is a continued fraction in the functions G. The recursion is terminated using G_{N-1} given in Eq. (33) or alternatively by defining $G_N \equiv 1$ and using Eq. (35). Finally, given $u_0=G_0u_{-1}$ along with u_0 and u_{-1} being known in terms of R, one has

$$R = \frac{G_0 e^{-ik_i a} - 1}{1 - G_0 e^{ik_i a}}. \tag{36}$$

In the high-frequency limit $\omega \to \omega_{\max}$ we have $\exp^{\pm ik_i a} \to -1$ once again yielding $R \to -1$ irrespective of the parameters used for the boundary region.

III. OPTIMIZATION OF DAMPED LAYERS

The analytical results from the previous section can be used to study the 1D chain in great detail, but their applicability to typical 3D systems of interest is more limited. In this section, we determine the optimal parameters for various types of boundary conditions using our analytical results as well as numerical techniques that will be introduced in this section.

We first apply the purely analytical results of the previous section to the PMMS/PML method[10,11] in order to determine optimal damping functions for that method. We then turn to MD (Ref. 17) simulations in both 1D and 3D. We employ Gaussian wave packets to sample $R(\omega)$ and then use this information to optimize the parameters of a particular boundary treatment. Our technique uses wave packets at many frequencies in the same simulation for efficient sampling.

Briefly, MD uses Newtonian dynamics with a numerical integration (in our case velocity Verlet) to simulate the particle trajectories subject to interatomic forces, see, e.g., Frenkel and Smit's text.[18] The first MD system we consider is a simple chain with a monatomic basis. The second system is a 3D silicon crystal with a "long" direction along the x axis and periodic boundary conditions in the y and z directions. The interface between atoms of interest and the atoms for the boundary condition lies in the y-z plane at the high x end of the simulation cell. For the excitations studied here, the 3D system is analogous to the 1D system although its dynamics are more complex.

Each optimization is used to validate the next. We use the optimal, analytically derived 1D damped boundary condition to validate the numerical results that are derived independently using the wave-packet method. With the wave-packet method we treat a richer set of configurations of the boundary layer and we carry over the best of these treatments to the 3D system. The 3D system is then used to test the applicability of this method to a more typical system of interest.

A. Minimization of the reflection coefficient

Here we define the optimum set of parameters $\mathcal{P}$ to be that set which minimizes $\overline{R^2}$, the average value of $R^2(\omega)$ over the Brillouin zone. This is certainly not the only possible definition; but it is the simplest which incorporates information about the performance of the boundary condition across the entire frequency spectrum. Alternatively, one may wish to focus on performance in a specific frequency band or one may consider thermal systems where it may be more appropriate to compute thermodynamic averages and incorporate the density of states.

Although $R(\omega)$ is known analytically for the 1D case, the integral of R over frequency is not, so we use numerical integration to determine $\overline{R^2}$ and to optimize this value as a

function of the free parameters. The actual values of R for any frequency ω may be determined directly from analytical expressions or using wave-packet MD simulation. Formally, the optimization problem is given by

$$\min_{\mathcal{P}} \overline{R^2} \equiv \min_{\mathcal{P}} \frac{1}{\omega_{\max}} \int_0^{\omega_{\max}} R^2(\omega) d\omega$$

$$\approx \min_{\mathcal{P}} \frac{1}{\sum_i \Delta\omega_i} \sum_i R^2(\omega_i) \Delta\omega_i, \tag{37}$$

where the rightmost expression is appropriate for the discrete sampling inherent in numerical integration methods. This is a nonlinear optimization which we perform with a local optimizer (a Newton-Raphson variant with a finite-difference Hessian). The solution to any local optimization scheme depends on the starting set of parameters. Hence, as we determine the optimal solutions for a sequence to treatments of increasing number of layers, we use the previous solution for a similar treatment with fewer layers (and parameters) which is subsumed in the current treatment. In addition, we bound the range of the parameters so that the critical time step of the explicit time integration is not affected by the boundary treatment.

Specifically, we can optimize with respect to a subset of the free parameters treated in Sec. II D: (a) damping only $\mathcal{P}=\{\gamma_i\}$, (b) interatomic spring plus per-atom damping $\mathcal{P}=\{\gamma_i,\kappa_{ij}\}$, (c) mass modification plus damping $\mathcal{P}=\{\gamma_i,m_i\}$, and (d) mass, stiffness and damping modification $\mathcal{P}=\{\gamma_i,m_i,\kappa_{ij}\}$. Since the harmonic oscillators representing the motion of the atoms in the lattice are coupled, each of these parameters, namely, mass, damping and stiffness, are independent. In terms of the linear system, mass scales the diagonal of the dynamical matrix, i.e., the left-hand side of Eqs. (27)–(29) reduced by mass and in matrix form, whereas interatomic spring stiffness also scales off-diagonal entries. We did not investigate the addition of harmonic well stiffness since it precludes $R^2(0)<1$, as discussed in Sec. II C, nor the addition of interatomic dampers. Interatomic dampers were discarded as a candidate modification mainly due to the fact they were not available in our target 3D code LAMMPS (Ref. 14) and are also relatively complex to implement due to the dependence on neighbor lists.

B. Perfectly matched layers

The free parameters of masses, stiffnesses, and damping constants provide considerable freedom in constructing a boundary condition. Indeed, the PMMS method using discrete PML[10,11] for the boundary region is a special case of this method. For the 1D chain, the PMMS boundary condition can be addressed analytically using the results of Sec. II. Following To and Li,[10] we use a so-called "damping function" d_i to define the parameters for layer i. Li *et al.*[11] present two possible boundary conditions that are local in time (and one that is nonlocal in time that we will not treat here). The boundary conditions differ by the choice of exponent in a scaling function used to modify the dynamics of the atoms in the boundary layer. For the simplest case, each boundary atom experiences a viscous force with damping constant $\gamma_i=md_i$ and we refer to this PMMS model as the "linear model." In the "quadratic model" the scaling is the square of that in the linear model and one has the nonzero parameters $\lambda_i=md_i^2$ and $\gamma_i=2md_i$. The mass is not considered variable in the PMMS method, so only a single mass m is defined for the chain. Likewise, the bond stiffness is held constant so that $\kappa_{ij}=\kappa$ for all layers. Given these definitions, the reflection coefficient as a function of the damping function is given by substitution into Eq. (36).

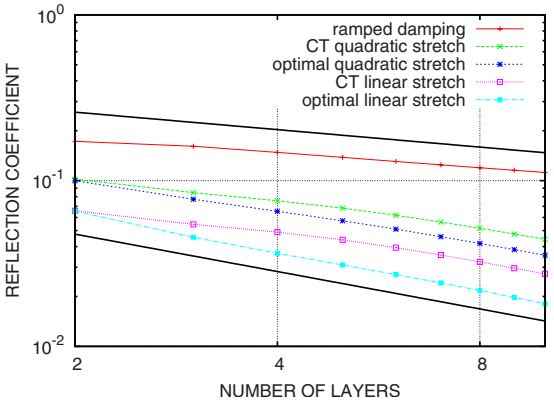

FIG. 4. (Color online) Average reflection coefficient $\overline{R^2}$ as a function of the number of boundary layers. The curves denoted with "CT" use the one parameter damping function, while the curves denoted as "optimal" have free parameters equal to the number of layers employed. The upper black trend line has an exponent of $-\frac{1}{3}$ and the lower trend line has an exponent of $-\frac{3}{4}$.

Given the analytical expression for $R(\omega)$, the *ad hoc* expressions for the damping function used in PMMS may be critically evaluated. The damping function $d_i=di^2$ used in PMML in the literature is due to Collino and Tsogka (CT),[19] and has a single free parameter d. We optimize this semiempirical damping function with respect to its free parameter for both the linear and quadratic stretching functions. An optimization is also carried out for each stretching function where no functional form is imposed on the damping function, i.e., each $\{d_i, i=1\ldots N\}$ is treated as a free parameter. The results of this optimization are shown in Fig. 4 and for comparison we show the optimal result for "ramped damping" where the damping constant varies linearly from the first to the last boundary atom $\gamma_i=\gamma i$. As seen in the figure, PML outperforms ramped damping, and the simplest method with linear stretching, which corresponds to each atom being damped with no other modification, yields the overall minimum of $\overline{R^2}$. As the number of layers N increases, we observe a power-law decay in $\overline{R^2}$ with $\overline{R^2}\sim N^{-0.76}$. For comparison, the CT damping function with linear stretching decays as $N^{-0.58}$, while the quadratic stretching decays as $N^{-0.64}$ in the optimal case and as $N^{-0.54}$ using the semiempirical damping function.

The optimal damping parameters as a function of the number of boundary layers N are shown in Fig. 5. Interestingly, the optimal damping constants approach $\bar{\beta}$ for the last (rightmost) boundary atom and approximately follow a linear, ramped damping profile for the rest of the boundary atoms. Alternately, it is apparent from Fig. 5(b) that the locus

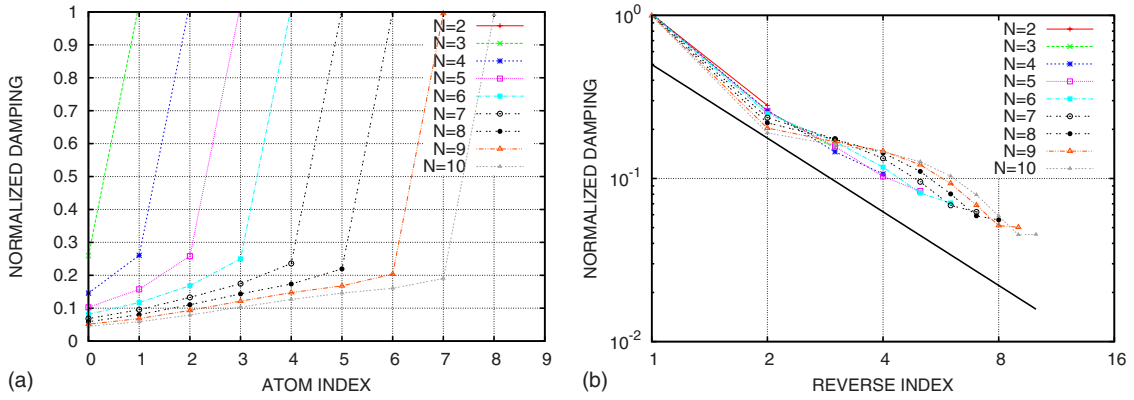

FIG. 5. (Color online) Optimal values of the PML damping parameters as a function of the number of boundary layers, (a) counting from the interface and (b) counting from the free end. The black trend line has an exponent of $-\frac{3}{2}$. Damping values γ_i have been normalized by $\bar{\beta}$.

of damping values decays with nearly power-law trend from the free end to the interface. However neither approximation is sufficiently accurate to allow us to ascertain the exact functional form of the optimal damping profile. The amplitude of the reflection coefficient as a function of frequency $R^2(\omega)$ is shown in Fig. 6. The effect of increasing N is to introduce additional local minima into the reflection coefficient, thereby lowering the average over frequency. Also, as N increases zeros in $R(\omega)$ appear near the high-frequency end of the Brillouin zone, as evidenced by the cusplike minima above normalized frequency 1.8.

C. Wave packets

For more complicated systems, the frequency response of the boundary can be determined via MD simulations using the multiple wave-packet method.[20] In this method, a set of wave packets, each with a central wave-vector $\vec{k}_i$ and central frequency ω_i, propagate at their group velocities $\frac{\partial\omega}{\partial\vec{k}}|_{\vec{k}=\vec{k}_i}$. In particular for a central wave-vector $\vec{k}_i$, normal mode amplitudes $\xi_{\vec{k}\zeta}$ given by

$$\xi^i_\zeta[\vec{k}_i + (\delta k_x)\hat{x}] = A_i e^{-\eta_0^2 \delta k_x^2} e^{-i[\vec{k}_i + (\delta k_x)\hat{x}]\cdot\vec{R}_i}, \tag{38}$$

are combined to generate a single wave packet.[21] The subscript ζ labels the phonon branch, which is fixed for a given

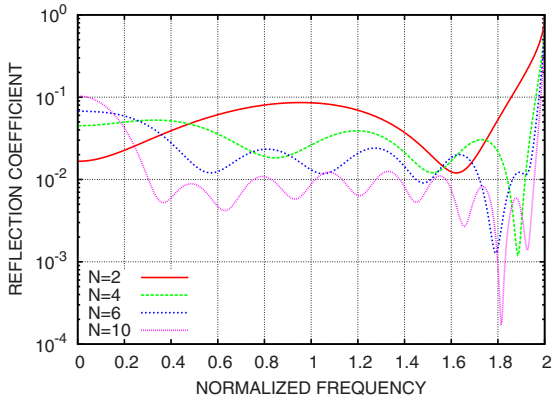

FIG. 6. (Color online) Reflection coefficient R^2 versus frequency ω for the optimal PML solution with 2, 4, 6, and 10 boundary layers. Frequency has been normalized by ω_0.

simulation. The arbitrary complex amplitude A_i determines the overall energy in the wave packet, and the δk_x-dependent phase shifts yield nonzero displacements and velocities localized about $\vec{R}_i$ in real space. The spatial extent of the localization varies inversely with η_0, which is chosen so that the wave packets do not overlap in frequency content. The initial atomic displacements are given by

$$\vec{u}_{il}(t=0) = \mathrm{Re}\sum_i \sum_{\vec{k},\zeta} \xi^i_\zeta(\vec{k})\vec{\epsilon}_{i\zeta}(\vec{k}) e^{i\vec{k}\cdot\vec{R}_l - i\omega_\zeta(\vec{k})t}|_{t=0}, \tag{39}$$

where $\vec{u}_{il}(t)$ represents the displacement for atom i in the unit cell labeled by l. The polarization vector $\vec{\epsilon}_{i\zeta}(\vec{k})$ is determined by diagonalizing the dynamical matrix of the bulk perfect crystal, as are the frequencies $\omega_\zeta(\vec{k})$, i.e., they are the eigenvectors and corresponding eigenvalues. The initial velocities $\vec{v}_{il}$ are given by the time derivative of Eq. (39) at $t=0$.

To determine the energy transmission coefficients as a function of branch and frequency, the final displacements and velocities after transmission through the interface are analyzed in terms of the normal modes of the perfect crystal lattice. The inverse of Eq. (39) is used to calculate the normal mode amplitudes $\xi_\zeta(\vec{k})$ after reflection from the boundary condition. Frequency space is binned with a bin centered on each central frequency of the multiple wave packets. The ratio of the energy reflected by the boundary in a given frequency bin to the initial energy in the same bin yields the discrete approximation to $R^2(\omega)$ sampled over branch ζ. Given that the group velocities of the wave packets depend on their central frequencies, care was necessary in assuring that the reflected packets all returned from the boundary within a given time window. In the following, the number of wave packets employed will be apparent from the number of points used in the graphs of $R^2(\omega)$.

D. Optimal damped layers

As mentioned at the beginning of this section, we use 1D MD together with the wave-packet method validated with analytical results in order to have a fully tested numerical optimization algorithm for our 3D system. To this end, we use a 1000 atom chain interacting with a Lennard-Jones (LJ)

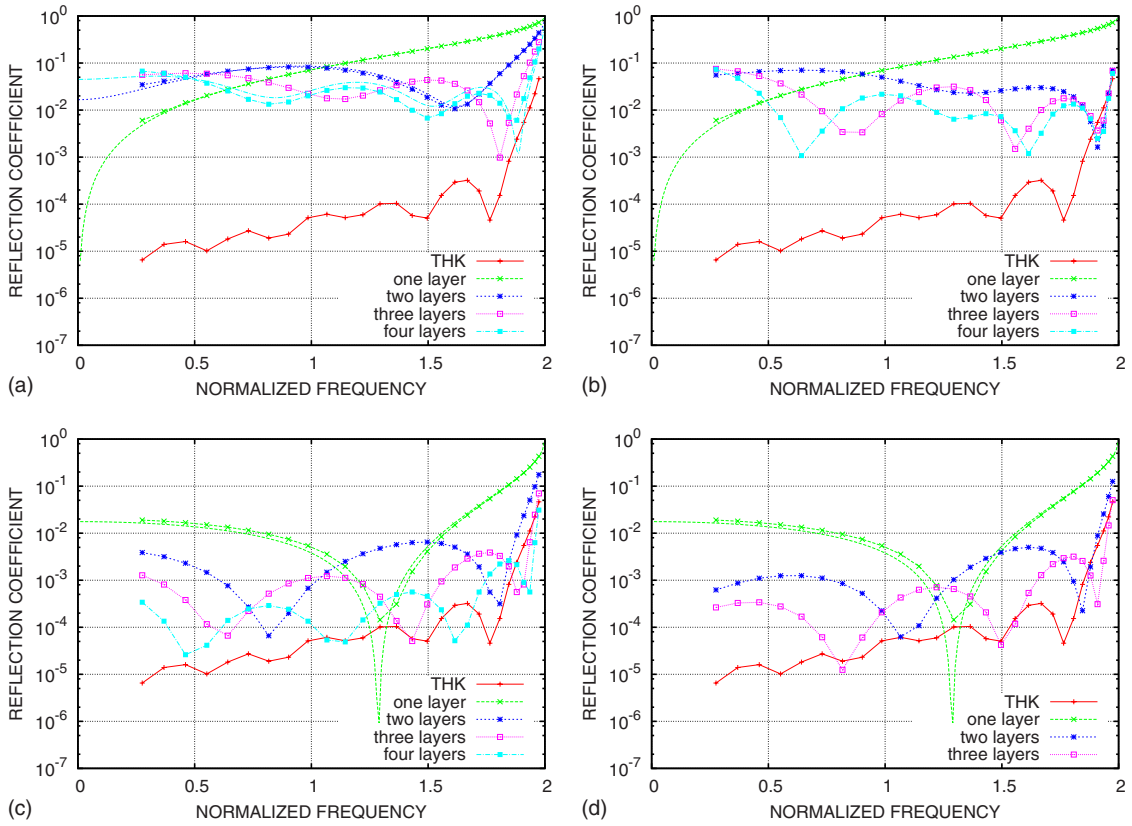

FIG. 7. (Color online) Reflection coefficient as a function of frequency for optimal damping and stiffness compared to the THK: (a) damping only, (b) spring and damping, (c) mass and damping, and (d) mass spring and damping. The curves that extend from normalized frequency 0 to 2 were generated from the analytic solution which was optimized independently.

potential ($\epsilon=1.0$ and $\sigma=1.0$) as an efficient test case for optimizing boundary treatments of fixed type and given number of layers. It is also an analogous system in all but the nonlinearity to the one analyzed in Sec. II and identical to the one treated in Sec. III B. The mass of all the atoms in the unmodified part of the chain was $m=1.0$. The zero temperature stiffness of the chain $\kappa=72.0$ gives a natural frequency $\omega_0=\sqrt{72.0}$ and $\omega_0/100\approx0.0012$ was chosen as a suitable time step. Wave packets with positive propagation directions were generated at the negative end of the (nonperiodic) chain, please refer again to the schematic in Fig. 2.

1. Optimal solutions

Figure 7 shows the spectral response of the optimal boundary conditions for the four types of damping layers described in Sec. III A, namely: (a) damping only, (b) interatomic spring plus per-atom damping, (c) mass modification plus damping, and (d) mass, stiffness, and damping modification. Corresponding analytical solutions for some of the treatments are plotted for comparison and to show the behavior at the ends of the Brillouin zone. It is evident from Fig. 7 that the numerical scheme replicates the analytical results in an acceptable fashion given the discrete frequency sampling. The error is seen to be negligible in most cases and greatest when the function being sampled has a large derivative with respect to frequency. This trend can be attributed to the finite spread in frequencies comprising a single wave packet, and the error may be reduced by reducing this spread at the expense of a larger MD system size. For reference, the response of THK with a 2000 step history and total reflection coefficient of $\overline{R^2}=0.0031$ is also shown. Clearly, the addition of stiffness or mass allows the optimal placement of zeros in the reflection spectrum $R^2(\omega)$ as evidenced by the cusplike minima. As more layers are added the zeros appear to be approximately evenly spaced across the Brillouin zone which effects a collocation of the reflection response to zero at discrete frequencies. For this particular system there appears to be a one-to-one correspondence with the number of zeros and the number of layers.

Table I summarizes the actual values determined by MD and numerical optimization for the various boundary treatments considered. As observed in Sec. III B, the set of parameters $\{\gamma_i\}$ for the damping-only optimal solutions does not display the linearity of a ramp but there is a marked increase in γ_i from nearly zero to a value nearly equal to $\bar{\beta}$ as the layer index i increases away from the interface and toward the free end. Comparing with Sec. III B, it is evident that the fully numerical approach has independently determined the optimal damping function for the linear PML stretching function, which provides validation of the MD wave-packet approach in the present context. The monotonic trend of $\{\gamma_i\}$ can also be seen in the mass-damping and mass-spring-damping treatments but not in the mass-spring boundary condition. From the data in Table I, we can see that the trend is nearly a power-law in the damping only and damp-

TABLE I. Optimal nondimensional parameters per layer. Masses m_i have been divided by the mass of a regular atom m, damping constants γ_i by $\bar{\beta}=\sqrt{m\kappa}$ and the stiffnesses κ_{ij} by the zero temperature stiffness of the LJ bonds κ. For comparison, a THK with a kernel of size 2000 has $\overline{R^2}=0.0031$.

N	$\overline{R^2}$	γ_0	m_0	$\kappa_{0,1}$	γ_1	m_1	$\kappa_{1,2}$	γ_2	m_2	$\kappa_{2,3}$	γ_3	m_3
1	0.1476	1.000										
2	0.0650	0.288			1.059							
3	0.0424	0.164			0.282			1.114				
4	0.0311	0.122			0.172			0.303			1.167	
1	0.1476	1.000										
2	0.0434	0.420		1.167	1.121							
3	0.0265	0.508		1.188	0.140		0.767	1.185				
4	0.0189	0.376		1.148	0.349		0.896	0.129		0.743	1.317	
1	0.0316	0.749	0.504									
2	0.0068	0.066	0.856		0.799	0.412						
3	0.0021	0.004	0.938		0.114	0.823		0.789	0.351			
4	0.0008	0.000	0.967		0.028	0.927		0.140	0.790		0.772	0.307
1	0.0316	0.749	0.504									
2	0.0040	0.168	0.893	1.086	0.823	0.392						
3	0.0013	0.000	0.985	1.039	0.199	0.843	1.086	0.798	0.328			

ing with mass adjustment, which is consistent with the findings of Sec. III B. From Fig. 8 we can see that, for the mass-damping treatment, as N increases the damping per layer approaches a similar power-law trend to a damping alone treatment albeit with a slightly faster decay. The mass, although clearly showing a smooth decay, is not well approximated by a power law (nor an exponential).

The table shows that the optimal solution for a single layer of damping is $\gamma=\bar{\beta}$, the velocity coefficient in the approximate β form of the THK, Eq. (7). It is also apparent from the table that changing the mass to (approximately) half the normal mass (and the damping to approximately $\frac{3}{4}\bar{\beta}$) leads to about five times better reflection coefficient than an optimal single layer treatment with damping alone. Consequently, the optimal PMMS methods treated here are not globally optimal, i.e., the variation of additional free parameters such as mass leads to significantly less reflection.

Figure 9 shows the convergence of $\overline{R^2}$ with increasing number of layers for the four types of treatments. It is apparent that the convergence rate of spring damping is comparable to damping alone and, similarly, mass-spring-damping is comparable to just mass damping, albeit with better leading coefficients. This observation is corroborated by fact that the optimal modified stiffnesses are near the value κ of the unmodified part of the chain. This first result is quite surprising since spring damping clearly affords the optimal placement of zeros in $R^2(\omega)$ that are absent in damping alone for a small number of boundary layers. Lastly, it is interesting to note that total reflection coefficient for the THK with a 2000 sample kernel is higher than the $N>2$ layer mass-damper and mass-spring-damper solutions mainly due to the high-frequency behavior which has been manipulated by placing a zero near $\omega_{\max}$.

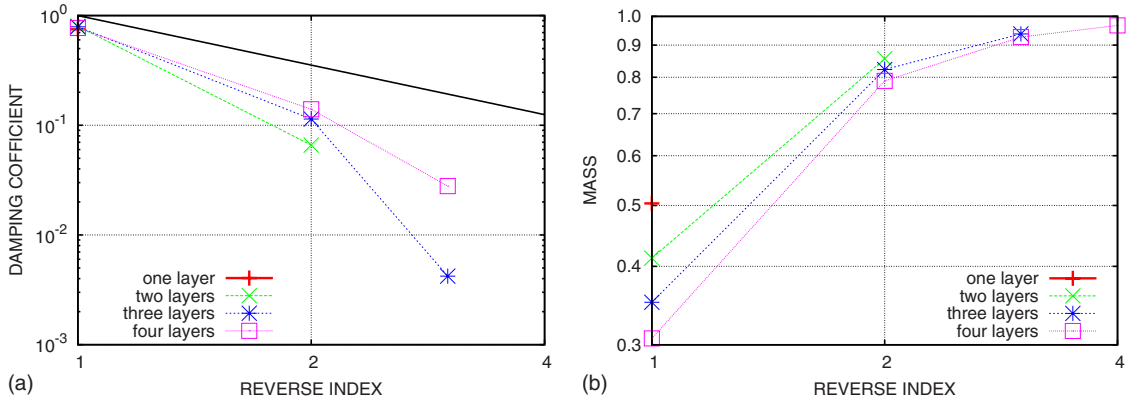

FIG. 8. (Color online) Optimal values of damping and mass for a mass-damper boundary layer counting from the free end. Damping values have been normalized by $\bar{\beta}$ and mass values by m. The black trend line has an exponent of $-\frac{3}{2}$ which facilitates comparison with Fig. 5.

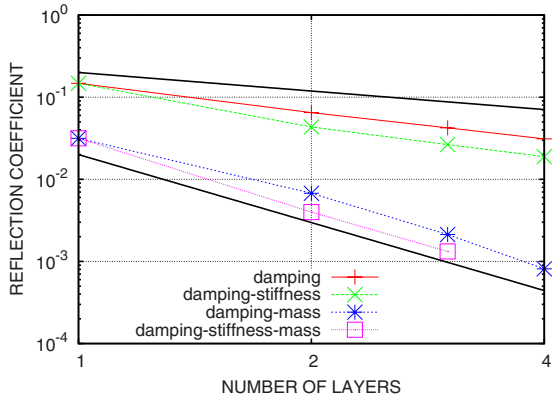

FIG. 9. (Color online) Average reflection coefficient $\overline{R^2}$ as a function of number of layers. The upper black trend line has an exponent of -1 and the lower trend line $-\frac{11}{4}$.

2. Shock

We tested our tuned boundary conditions with a broadband disturbance created by a large amplitude velocity impulse in the nonlinear regime, where the amplitude of the resultant shock was roughly one hundred times that of the wave packets. This simulation was chosen over, for example, a fracture simulation since it was much simpler to construct and analyze while at the same time replicating most of the qualitative features of an isolated fracture event. We compared the optimal $N=3$ layer mass-spring-damper treatment (refer to Table I) to a THK with a 2000 sample kernel.

Figure 10(a) shows the frequency response of the THK and optimal damping. A fast Fourier transform (FFT) of the incident velocity waveform was taken after shock developed but before it interacted with the boundary. Similarly, FFTs of the reflected waveform were taken after all the significant part of the wave form had left the vicinity of the boundary. Figure 10(a) clearly reflects the relationship $E_{reflected}(\omega)=R^2(\omega)E_{incident}(\omega)$ and that both treatments are ineffective at removing the high-frequency content with nearly zero group velocities.[27] Fig. 10(b) shows the temporal response of the THK and damped layers to the velocity impulse, where both are characteristic of the THK's β kernel (4) damped oscillations. Clearly, the exponential envelope of the layer solution falls inside the envelop of the THK. As a point of reference for this particular system, the THK treatment took 2.941 s to complete 100 000 time steps, compared to 0.990 s for the layers solution which represents approximately a factor of 3 speed up for essentially the same performance.

E. Optimal layers in a three-dimensional system

In this simulation, we employ a $500\times1\times1$ unit cell silicon system with Stillinger-Weber interactions.[22] Although the long direction of the system draws comparison to the 1D chain, the potential includes three body interactions and the silicon lattice has a polyatomic basis, leading to the presence of optical branches in the phonon spectra. We consider the response of the boundary to longitudinal acoustic (LA) wave packets which have normal incidence on the y-z boundary plane, i.e., the incident wave packets have central wave vectors of the form (k_x00), yielding a dispersion relation functionally equivalent to the 1D chain. Although the dispersion relation of the 3D system is much richer than the 1D system, we optimize $\overline{R^2}$ only over the LA branch $\omega(k_x00)$ and note that we do not observe conversion between branches as wave packets scatter off the boundary. In this case we only consider damping or mass and damping modification per quarter cell layer, since these boundary treatments are as effective as those that modify the stiffness and required no modification of LAMMPS.[14]

1. Optimized layers

Figure 11 shows the frequency response of the optimal filters which are tuned for the full LA spectrum. From Fig. 11 it is not apparent that the reflection coefficient for any of the boundary layer treatments is approaching one at the high-frequency end of the Brillouin zone as in the one-dimensional case without a basis, although this may just be an artifact of our ability to resolve frequencies at the ends of the Brillouin zone with wave packets. Clearly, mass damping is more effective across the full spectrum than damping alone due to adding zeros of the reflection coefficient near

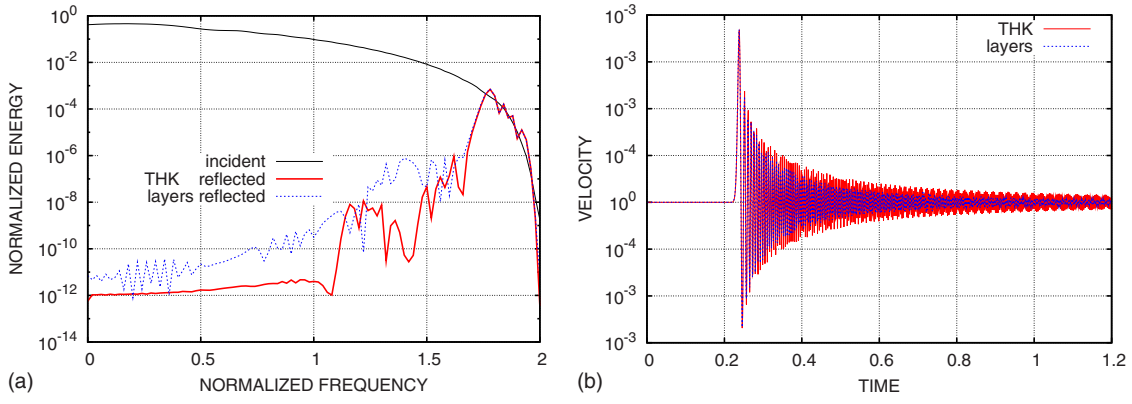

FIG. 10. (Color online) Shock incident and reflected energy normalized by the total energy of the (a) incident waveform and (b) temporal response for the optimal three layer mass-spring-damper boundary condition and a 2000 step long THK. Frequency has been normalized by ω_0.

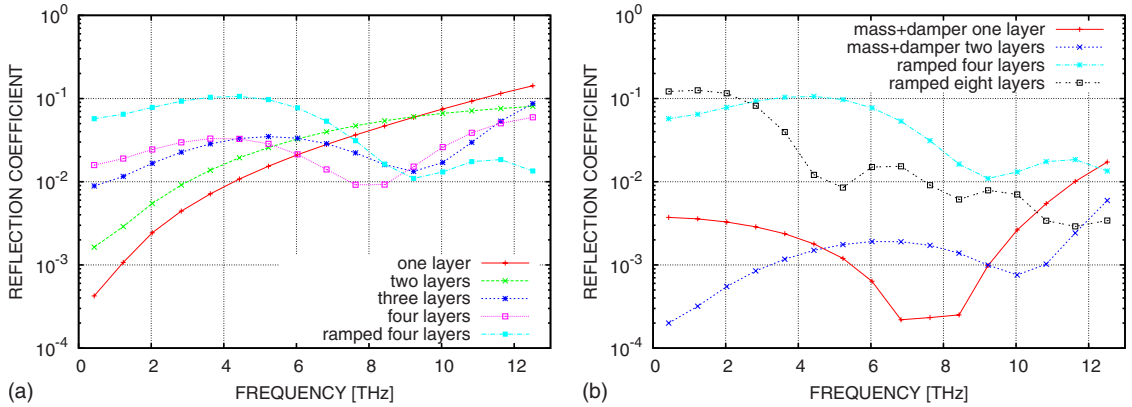

FIG. 11. (Color online) Reflection coefficient as a function of frequency for optimal damping and mass compared to ramped. (a) damping only, (b) mass and damping.

the middle of the Brillouin zone. This fact is demonstrated by the convergence rates shown in Fig. 12. The mass-damping treatment is also more effective than an optimized linearly ramped damping, which has a convergence rate comparable to optimal per layer damping. However, unlike per layer optimized treatments which tend to be more effective at lower frequencies, ramped damping is particularly effective at damping high frequencies. Table II shows that the trends in the optimal parameters are similar but not quite the same as the 1D system of Sec. III D summarized in Table I. In fact, the optimal damping for this system is not always monotonic with increasing layer index i. Figure 12 also shows that the rates of convergence for similar boundary treatments are also substantially lower in this quasi-3D setting.

2. Shock

As in Sec. III D 2, we generate a velocity impulse at the low x end of the system that propagates toward the damped boundary at the high x end as a test of the ability our tuned layer to handle a broadband disturbance characteristic of a fracture event. Figure 13 shows discrete Fourier transforms of the displacement waveform after it has reflected from the end for both: (a) an optimal two layer mass-damper treatment and (b) a simple fixed end condition. The fixed end clearly preserves the frequency content of the waveform whereas the damped layer decreases the main displacement components significantly. The reflection coefficient obtained from this waveform is, at least qualitatively, consistent with the frequency response obtained from the wave packets, as shown in Fig. 11. Both the LO and LA branches show similar behavior despite the fact that the boundary treatment was only tuned to LA wave packets. Another observation of interest is:there are many more zeros to the reflection response than would be expected from the number of layers and the 1D results of Sec. III D (In 1D we observed one zero per layer for low number of layers of mass damping).

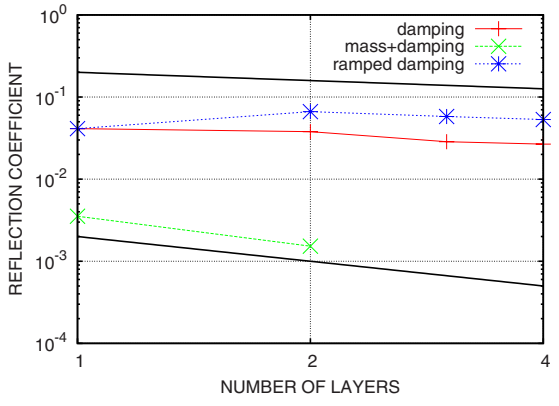

FIG. 12. (Color online) Total reflection coefficient as a function of number of layers. Upper black trend line exponent $-\frac{1}{3}$, lower trend line -1.

IV. DISCUSSION

We have provided analysis and a numerical methodology to create efficient, effective, nearly reflectionless boundary treatments. The methodology can be trivially extended to band-pass filtering for the low-frequency/high-frequency split necessary for multiscale domain decompositions. The one obvious downside to our approach is that it is apparently dependent on the particular impedance properties of the system of interest and in principle requires an optimization step to determine effective parameters for damping. However,

TABLE II. Optimal nondimensional parameters per layer. Masses m_i have been divided by the mass of a regular atom m, damping constants γ_i by $\bar{\beta}$. For reference, the optimal ramped solution are: one layer $\gamma=1.000$ with $\overline{R^2}=0.0412$, two layers $\gamma=0.8602$ with $\overline{R^2}=0.0664$, three layers $\gamma=0.7493$ with $\overline{R^2}=0.0578$, four layers $\gamma=0.7234$ with $\overline{R^2}=0.0532$.

N	$\overline{R^2}$	γ_0	m_0	γ_1	m_1	γ_2	m_2	γ_3	m_3
1	0.0412	1.000							
2	0.0379	0.099		1.020					
3	0.0286	0.164		0.084		1.000			
4	0.0267	0.076		0.168		0.081		1.006	
1	0.0035	0.917	0.555						
2	0.0015	0.073	1.031	0.936	0.575				

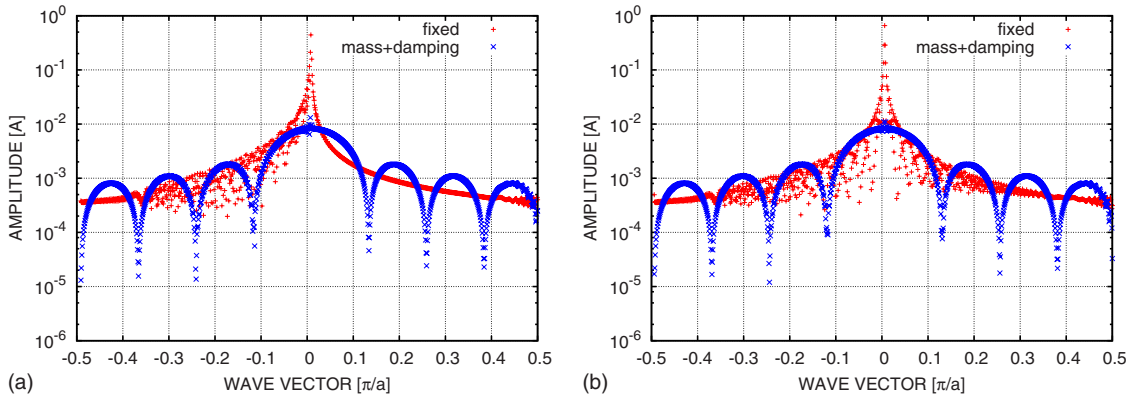

FIG. 13. (Color online) Shock in Si (a) LA branch and (b) LO branch. The wave vector has been normalized by π over the lattice constant $a=5.43094$ Å.

this step may at worst be performed once for a system which is used for many different simulations, i.e., for Stillinger-Weber silicon with an (001) boundary plane. Also, effective but not optimal boundary conditions may be employed without the optimization process, by applying known parameters from one system to a similar system. Although we have not explored the sensitivity of the parameters in the optimal solutions, we conjecture that the reflection properties are not extremely sensitive to the exact values of damping, additional mass, and interatomic stiffness per layer. Moreover, the clear trend in optimal PMMS solutions for the 1D system suggest a better-performing alternative to the current damping functions commonly used in that method. With that being said it seems practical to construct a useful damped boundary treatment by just understanding where added mass or stiffness places zeros in the reflection spectrum in the frequency band of interest.

One perspective that may help in this endeavor is the idea that each of the damped boundary layers governed by second order ordinary differential equations characteristic of coupled, damped harmonic oscillators which can be interpreted in the context of a sequence of second order filters. In the optimization problem, we adjust mass, damping, and stiffness of the exterior layers in order to effect zeros in the transfer function defined by the reflection coefficient $R(\omega)$ in analogy with the design of a filter. Although there is no history or convolution explicitly in this type of treatment, the propagation of a waveform through a finite number of layers adds delays that are also characteristic of a sequential filter. Basic filter design relies on "zero-pole" analysis of the transfer function $R(\omega)$ which starts with a factorization of the numerator and denominator of the transfer function. We will pursue this analysis this in future work. Like all other treatments known to the authors, our analysis is done in continuous time and connects to analog filters. In future work we intend to explore the discrete time aspects of the MD reflectionless boundary condition problem.

The analogy between wave propagation and signal propagation is actually an old one going back to Brillouin.[23] Specifically Brillouin states that a boundary layer with half the mass of the normal chain leads to a vanishing real part of impedance, a fact that our results corroborate, refer to Table I. In the event that a full optimization is not warranted for the system of interest, a single layer of damping with half the mass and a damping coefficient of approximately the spring constant times the natural frequency should be effective as a nonreflecting boundary condition. For a multiple-layer boundary condition, the optimal linear PML may be used where the final damped atom is damped by the same value suggested for a single layer and a ramped damping profile is used for all other layers.

We have not touched on the issues implicit in truly three-dimensional configurations with waveforms with non-normal incidence, nor on lattices with more than nearest-neighbor interactions. We leave these topics for future work. Extension of this work to finite-temperature systems should be relatively straightforward since the creation of the damping kernel or its efficient approximation, as in this work, is independent of the generation of the random force term used in generalized Langevin treatments to maintain the temperature at the boundary. Of course the fluctuation-dissipation theorem does link the two together and establishing this connection precisely for the proposed represents the primary challenge.

ACKNOWLEDGMENTS

This work was funded by the Engineering Science Research Foundation program at Sandia National Laboratories and its support is gratefully acknowledged. Sandia is a multiprogram laboratory operated by Sandia Corporation, a Lockheed Martin Co., for the United States Department of Energy under contract No. DE-ACO4-94AL85000.

*rjones@sandia.gov
†chris.kimmer@louisville.edu

[1] B. Engquist and A. Majda, Commun. Pure Appl. Math. **32**, 313 (1979).
[2] J. Bérenger, J. Comput. Phys. **114**, 185 (1994).
[3] S. A. Adelman and J. D. Doll, J. Chem. Phys. **64**, 2375 (1976).
[4] H. Mori, Prog. Theor. Phys. **34**, 399 (1965).
[5] G. Wagner and W. Liu, J. Comput. Phys. **190**, 249 (2003).
[6] W. Cai, M. de Koning, V. V. Bulatov, and S. Yip, Phys. Rev. Lett. **85**, 3213 (2000).
[7] E. Karpov, G. Wagner, and W. Liu, Int. J. Numer. Methods Eng. **62**, 1250 (2005).
[8] W. E and Z. Huang, Phys. Rev. Lett. **87**, 135501 (2001).
[9] X. Li and W. E, Comm. Comp. Phys. **1**, 136 (2006).
[10] A. C. To and S. Li, Phys. Rev. B **72**, 035414 (2005).
[11] S. Li, X. Liu, A. Agrawal, and A. C. To, Phys. Rev. B **74**, 045418 (2006).
[12] M. N. Guddati and S. Thirunavukkarasu, J. Comput. Phys. **228**, 8112 (2009).
[13] J. Z. Yang and X. Li, Phys. Rev. B **73**, 224111 (2006).
[14] S. Plimpton, J. Comput. Phys. **117**, 1 (1995).
[15] C. Steinbrüchel, Z. Phys. B Condens. Matter **24**, 293 (1976).
[16] H. Mori, Prog. Theor. Phys. **33**, 423 (1965).
[17] M. Allen and D. Tildesley, *Computer Simulation of Liquids* (Oxford University Press, New York, 1987).
[18] D. Frenkel and B. Smit, *Understanding Molecular Simulation* (Academic Press, San Diego, 2001).
[19] F. Collino and C. Tsogka, Geophysics **66**, 294 (2001).
[20] C. Kimmer, S. Aubry, A. Skye, and P. K. Schelling, Phys. Rev. B **75**, 144105 (2007).
[21] P. K. Schelling, S. R. Phillpot, and P. Keblinski, J. Appl. Phys. **95**, 6082 (2004).
[22] F. H. Stillinger and T. A. Weber, Phys. Rev. B **31**, 5262 (1985).
[23] L. Brillouin, *Wave Propagation in Periodic Structures*, 2nd ed. (Dover, New York, 1953).
[24] This approach differs from the original work of E and Huang[8] where only the reflection coefficient in the neighborhood of zero frequency was used to determine the damping coefficients.
[25] By looking at the reflection minimization problem as a generic optimization problem, this behavior can be understood. An unmodified, fixed boundary gives a reflection function of one for all frequencies. When zeros are added by damping/stiffness/mass modification, these zeros act as collocation points for the reflection function. Since it appears that each damping element adds a single zero at an independent frequency, the optimal solution for a finite number of collocations in minimizing a function that responds in a regular and uniform fashion is to have those collocation points be regularly spaced across the function's finite range.
[26] We are not considering thermalized lattices in this work.
[27] In a finite-temperature simulation these frequencies would be interpreted as thermal vibrations and arguably demand separate treatment.